Accelerating relaxation through Liouvillian exceptional point

Yan-Li Zhou,[1,2,3,*] Xiao-Die Yu,[4] Chun-Wang Wu,[1,2,3] Xie-Qian Li,[1] Jie Zhang,[1,2,3] Weibin Li,[5,†] and Ping-Xing Chen[1,2,3,‡]

[1]*Institute for Quantum Science and Technology, College of Science, National University of Defense Technology, Changsha 410073, China*
[2]*Hunan Key Laboratory of Mechanism and technology of Quantum Information, Changsha 410073, China*
[3]*Hefei National Laboratory, Hefei 230088, Anhui, China*
[4]*College of Science, National University of Defense Technology, Changsha 410073, China*
[5]*School of Physics and Astronomy, and Centre for the Mathematics and Theoretical Physics of Quantum Non-equilibrium Systems, University of Nottingham, Nottingham NG7 2RD, United Kingdom*

(Received 22 May 2023; accepted 22 September 2023; published 11 October 2023)

We investigate speeding up of relaxation of Markovian open quantum systems with the Liouvillian exceptional point (LEP), where the slowest decay mode degenerates with a faster decay mode. The degeneracy significantly increases the gap of the Liouvillian operator, which determines the time scale of such systems in converging to stationarity and thus accelerates the relaxation process. We explore an experimentally relevant three-level atomic system whose eigenmatrices and eigenspectra are obtained completely analytically. This allows us to gain insights into the LEP and examine the respective dynamics with details. We illustrate that the gap can be further widened by Floquet engineering, which further accelerates the relaxation process. Finally, we extend this approach to analyze laser cooling of trapped ions, where vibrations (phonons) couple to the electronic states. An optimal cooling condition is obtained analytically, which agrees with both existing experiments and numerical simulations. In this paper, we provide analytical insights into understanding LEP as well as controlling and optimizing the dissipative dynamics of atoms and trapped ions.

DOI: 10.1103/PhysRevResearch.5.043036

I. INTRODUCTION

Open quantum systems coupled to environments will relax toward a stationary state. The relaxation processes have rich properties from both dynamic and thermodynamic perspectives. Often, an important question is to control the relaxation time [1–4], for instance, on a time scale as short as possible [see Fig. 1(a)]. This problem is of great relevance to cases where one is concerned with properties of stationary states, such as ground state laser cooling [5–10], or aims to generate quantum states for quantum applications [11–14].

Starting from an arbitrary initial state, the relaxation time scale is largely characterized by the slowest decay mode of the Liouvillian operator. The gap is defined as the modulus of the real part of its eigenvalue λ_1 [15–17], as depicted in Fig. 1(b). Therefore, relaxation speeding is achieved through increasing the gap. An alternative approach to speed the relaxation is offered by the so-called Mpemba effect [18–23], where a unitary operation on the initial pure state removes its overlap with the slowest decaying mode [1,2]. This transformation can be exactly constructed provided that the initial state is a pure state.

In this paper, we show that, for an arbitrary initial state, if the slowest decay mode and its corresponding eigenvalue coalesce with a faster decay mode, one can maximize the gap and thus accelerate dynamics to reach stationary states. Here, we exploit the nature of exceptional points (EPs), where two or more eigenvalues of a non-Hermitian operator and their corresponding eigenvectors coalesce [24,25]. The origin of non-Hermiticity is the coupling between the system and the environment. A Liouvillian superoperator, which captures the time evolution of an open quantum system, is non-Hermitian. Therefore, it can exhibit EPs [referred to as Liouvillian EPs (LEPs)] [24,26]. Properties of LEPs, with diverse unusual effects, have attracted considerable current attention [27–29], such as dissipative phase transition [30–32], the non-Hermitian skin effect [33], signatures of LEPs in the dynamics [34–36], in a continuous variable system [37], and in state preparation [38]. The authors of Ref. [35] have uncovered the existence of LEPs in the dynamics of a quantum thermal machine in the form of critical decay toward the steady state, in analogy to critical damping in a harmonic oscillator. In Ref. [29], the authors have studied the optimization of dynamics in the context of LEPs. For a two-level quantum system, they have showed the optimum relaxation rate is linked with LEPs, and a significant speedup can be achieved with a slight compromise in the target state purity. These studies show that LEPs play an important role in a variety of optimization problems [39–41].

*ylzhou@nudt.edu.cn
†weibin.li@nottingham.ac.uk
‡pxchen@nudt.edu.cn

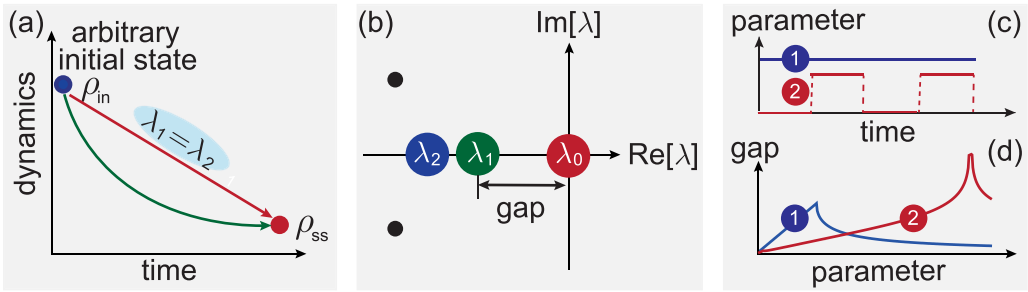

FIG. 1. (a) For an open quantum system with an arbitrary initial state, the time scale of approaching the final stationary state ρ_{ss} is related to the slowest decay mode (with eigenvalue λ_1) of the Liouvillian superoperator. By tuning the parameter of the system near the Liouvillian exceptional points (LEPs), where both the slowest decaying mode and the corresponding eigenvalue are merged with a faster decaying mode and the corresponding eigenvalue (for instance, λ_2), the system dynamics approaches the stationary state in a much faster way. (b) This feature is evident from the Liouvillian spectrum. The stationary state ρ_{ss} is characterized by the largest eigenvalue $\lambda_0 = 0$. The other eigenvalues, characterizing the decay modes, have a nonpositive real part and always appear as complex conjugates. The Liouvillian spectral gap ($g = -\mathrm{Re}[\lambda_1]$) determines the relaxation time scale and could reach its maximum value at the LEP. (c) and (d) The gap at the LEP can be further increased by the Floquet method (red line). In contrast with the static case (blue line), the gap under time-periodic modulation can be significantly increased, which means that relaxation process will be accelerated by applying the Floquet method.

Here, we show that, when the stationary state of the system is unique and independent of system parameters, one can set the parameters at the LEP to speed up the relaxation process significantly. The basic mechanism underpinning this paper is based on the fact that, at LEPs, both the slowest decay mode and corresponding eigenvalue coalesce with a faster decay mode and corresponding eigenvalue. In addition, we find that relaxation processes can be further accelerated by periodically modulating the dissipation strength, i.e., the Floquet modulation can overcome the gap limit of the static case and realize faster relaxation [see Figs. 1(c) and 1(d)]. We apply our approach to analyze ground-state laser cooling based on sideband transitions and electromagnetically induced transparency (EIT) and obtain the optimal conditions analytically in the context of LEPs. Therefore, in this paper, we reveal the importance of LEPs in practical applications and provide insights into seeking optimal conditions in quantum control of open quantum systems.

This paper is organized as follows. In Sec. II, we introduce the master equation of the Markovian open quantum systems. A general framework that connects to its dynamics and eigenmatrices of the Liouvillian superoperator is provided. This provides an intuitive picture to understand the relaxation and the gap. In Sec. III, we study the dynamics of dissipative three-level system. Eigenmatrices and eigenvalues of the corresponding Liouvillian superoperator are obtained analytically. Based on the analytical calculation, we reveal that the relaxation toward to stationary state can be accelerated by exploiting static and Floquet-modulated LEPs. Next, in Sec. IV, applications for ground-state laser cooling are demonstrated. Two experimentally relevant scenarios, i.e., sideband cooling and EIT cooling, are examined. Optimal cooling conditions are obtained at corresponding LEPs. We conclude in Sec. V.

II. LIOUVILLIAN GAP, DYNAMICS, AND LEP

We consider an open quantum system evolving under Markovian dynamics, governed by master equation $\dot{\rho}(t) = \mathcal{L}\rho(t)$, where the generator $\mathcal{L}$, normally called the Liouvillian superoperator, has the form [42,43]:

$$\mathcal{L}\rho = -i[H,\rho] + \sum_{\alpha}\left(J_\alpha \rho J_\alpha^\dagger - \frac{1}{2}\{J_\alpha^\dagger J_\alpha, \rho\}\right). \tag{1}$$

Here, $\rho(t)$ is the state of the system at time t, H is the system Hamiltonian, and J_α are quantum jump operators which provide coupling of the system to the environment. Since the Liouvillian $\mathcal{L}$ acts linearly on $\rho(t)$, one can obtain information about the relaxation in terms of its eigenmatrices R_i and the corresponding complex eigenvalues λ_i via the relation $\mathcal{L}R_i = \lambda_i R_i$. Note that, due to the Hermiticity preserving of $\mathcal{L}$, if λ_i is complex, λ_i^* must also be an eigenvalue of $\mathcal{L}$ [1,26,31,44]. Therefore, the eigenvalues are symmetrically distributed with respect to the real axis, as shown in Fig. 1(b).

The stationary state of the system under consideration is then given by the density matrix ρ_{ss} such that $\mathcal{L}\rho_{ss} = 0$, i.e., $\rho_{ss} = R_0$, which corresponds to the zero eigenvalue $\lambda_0 = 0$ and is independent of the initial state. If the eigenvalues are ordered by decreasing their real parts, it is known that the negative real parts of the eigenvalues [45], $\mathrm{Re}[\lambda_{i>0}] < 0$, determine the relaxation rates of the system toward the nonequilibrium stationary state, and the corresponding eigenmatrices $R_{i>0}$ are called decay modes [16,46], while the imaginary parts describe the oscillatory processes which may take place. We can then write the time dependence of the density operator from an initial state ρ_{in} as

$$\rho(t) = e^{\mathcal{L}t}\rho_{\mathrm{in}} = \rho_{ss} + \sum_{i\geqslant 1} a_i e^{\lambda_i t} R_i, \tag{2}$$

where $a_i = \mathrm{Tr}[L_i\rho_{\mathrm{in}}]$ are coefficients of the initial state decomposing into the eigenmatrices of $\mathcal{L}^\dagger$ with $\mathcal{L}^\dagger L_i = \lambda_i^* L_i$. Here, R_i and L_i are referred as right and left eigenmatrices (eigenmodes), respectively, and can be normalized by $\mathrm{Tr}[L_i R_j] = \delta_{ij}$. The trace preservation of the dynamics implies that $\mathrm{Tr}[\rho(t)] = \mathrm{Tr}[\rho_{ss}] = 1 = \mathrm{Tr}[L_0 R_0]$, and thus, L_0 is the identity ($L_0 = I$). It also implies that $\mathrm{Tr}[R_{i\geqslant 1}] = 0$, which means other right eigenmatrices do not correspond to quantum states. A particularly interesting case is when

eigenvalue λ_i is real, where the corresponding eigenmatrix can be diagonalized [31]. We can rewrite it as the superposition of eigenstates from the diagonalization [31]:

$$R_i \propto R_i^+ - R_i^-, \tag{3}$$

with

$$R_i^+ = \sum_n^{p_n \geqslant 0} p_n^i |\psi_n^i\rangle\langle\psi_n^i|,$$
$$R_i^- = \sum_n^{p_n < 0} p_n^i |\psi_n^i\rangle\langle\psi_n^i|, \tag{4}$$

where $|\psi_n^i\rangle$ are eigenvectors of R_i with eigenvalues p_n^i. With this definition, $R_i^{\pm}$ are arranged to proper density matrices. If λ_i is complex, one can define a pair of eigenmatrices $R_i + R_i^\dagger$ and $i(R_i - R_i^\dagger)$; then their corresponding eigenvalues are real (i.e., the real part of λ_i). This allows us to diagonalize their new eigenmatrices.

A fundamental role in the system dynamics is played by R_1, which possesses the slowest decay rate $-\mathrm{Re}[\lambda_1]$ on the condition $a_1 \neq 0$. Then the Liouvillian gap, defined by $g = -\mathrm{Re}[\lambda_1]$, is thus an important quantity determining the time scale of the final relaxation to the stationary state [15,47]. Consequently, for long times, one has

$$||\rho(t) - \rho_{ss}|| \propto e^{-gt}, \tag{5}$$

where $||A|| = \sqrt{\mathrm{Tr}[AA^\dagger]}$ is the Hilbert-Schmidt distance.

If the slowest decay mode $\lambda_1(R_1)$ coalesces with a faster decay mode [for instance, $\lambda_2(R_2)$] at the LEP, the maximum gap (i.e., the optimum convergence rate) is achieved naturally. This means that we can actively engineer the relaxation to the stationary state with the fastest convergence rate by tuning the parameters of the system approaching to LEP. Generally, this steering will also change the stationary state to which the system relaxes. However, in certain quantum applications, the dissipation inevitably leads the system into a dark state or manifold [48], or the target stationary state might be parameter insensitive [11]. In those cases, long relaxation time scales become impractical or even harmful to the coherence. Therefore, quickly approaching the steady state becomes necessary in these applications. In the next section, we demonstrate that our LEP speed-up approach is viable in those cases.

III. ANALYTICAL LEP THEORY OF DISSIPATIVE THREE-LEVEL SYSTEM

A. The model

Consider a simple dissipative three-level system of Fig. 2(a) [48]. The state $|b\rangle$ resonantly couples to state $|c\rangle$ with Rabi frequency Ω; state $|c\rangle$ decays to state $|a\rangle$ by emitting a photon with decay rate γ. For the model under consideration, we have the Hamiltonian:

$$H = \frac{\Omega}{2}(|b\rangle\langle c| + |c\rangle\langle b|), \tag{6}$$

and a jump operator $J = \sqrt{\gamma}|a\rangle\langle c|$. This process results in state $|b\rangle$ decoupled from the coherent collective evolution and eventually decaying to the stationary state $|a\rangle$, which

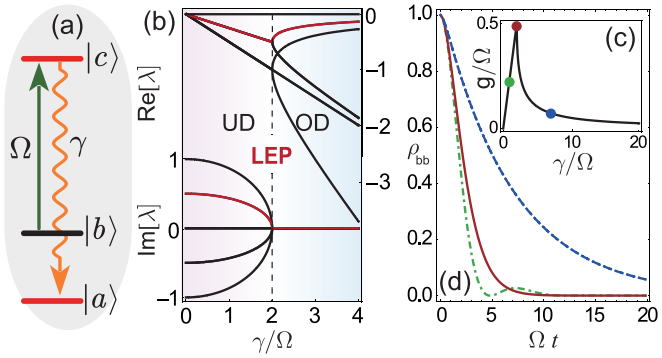

FIG. 2. (a) Schematic of the system; γ denotes the emission rate of the $|c\rangle$ level to $|a\rangle$ level, and Ω denotes the coupling rate from an resonant drive between transition $|b\rangle$-$|c\rangle$. (b) Real and imaginary parts of the Liouvillian spectra of the three-level system shown in (a). The red solid lines correspond to λ_1, and the Liouvillian exceptional point (LEP) is indicated with a vertical dashed line. (c) The Liouvillian gap as a function of γ/Ω. (d) Relaxation process. The system decays exponentially to the final stationary state. The numerical integration is performed in the underdamped (UD) regime with $\gamma = \Omega$ (dot-dashed green line), in the overdamped (OD) regime with $\gamma = 7\Omega$ (dashed blue line), and in the LEP with $\gamma = 2/\Omega$ (solid red line).

is obviously parameter independent. Qualitatively, there will be competition between the reversible coherent coupling between $|b\rangle \leftrightarrow |c\rangle$ at frequency Ω and the population loss of $|c\rangle$ at a rate γ. If there are no thermal photons to drive the $|a\rangle \rightarrow |c\rangle$ transition, the decay to $|a\rangle$ is unidirectional, and hence, $|a\rangle$ is a dark state. This simple model has been applied to engineer quantum states in all the forerunning platforms for quantum information processing [11,49–55]. Furthermore, as we show below, phonon ground-state cooling provides a closely related example of this model [5,56–58].

B. The Liouvillian spectra and LEPs

For this level system, the stationary state of the system is always $|a\rangle$, no matter how the initial state and parameters of the system change. If the goal is to prepare or use this state for related applications, it is unnecessary and even harmful to wait for long relaxation time scales. In this instance, the most practical construction is to set the optimal parameters to ensure approaching the stationary state on a time scale which is as short as possible. It can be obtained quantitatively by solving the spectrum of Liouvillian superoperator $\mathcal{L}$, as shown in Fig. 2(b), and it is $\{0, -(\gamma \pm \kappa)/4, -(\gamma \pm \kappa)/2, -\gamma/2\}$, with $\kappa = \sqrt{\gamma^2 - 4\Omega^2}$. Consequently, the spectrum gap is

$$g = \mathrm{Re}\left[\frac{1}{4}(\gamma - \kappa)\right]. \tag{7}$$

Equation (7) highlights different trends in the function of γ/Ω, as shown in Fig. 2(c). When $\gamma < 2\Omega$, the gap ($= \gamma/4$) is linearly increased with γ until $\gamma = 2\Omega$, i.e., the special LEP. If $\gamma > 2\Omega$, on the other hand, the gap will decrease with γ/Ω which provides a tunable dissipation channel [12,13,36], and recently, it has been widely used to simulate

parity-time ($\mathcal{PT}$)-symmetric Hamiltonians with postselection of the jump results [27,36,54,59]. Obviously, the gap reaches the maximum value $g_{\max} = \gamma/4 = \Omega/2$ at the LEP. As shown in Fig. 2(d), the optimum relaxation rate is linked with LEPs, and a significant speedup of our model can be achieved by tuning the parameters approaching the LEP. The idea of EPs being related to the critical decay rate appears in the non-Hermitian Hamiltonian system [25] and extends to the non-Hermitian Liouvillian [29,35,37,60]. In Ref. [35], authors discuss that the optimal relaxation rate linked with LEPs is rooted in the time-polynomial terms appearing in the dynamics at the LEP, where it behaves as a critical damping making the boundary between the underdamped (UD) to the overdamped (OD) dynamics in analogy with a classical damped harmonic oscillator [11,26]. From a different perspective, we show this property stems from the slowest decay eigenmode coalescing with a faster one at the LEP.

As shown in Fig. 2(b), structures $\{-(\gamma \pm \kappa)/4\}$ and $\{-(\gamma \pm \kappa)/2, -\gamma/2\}$ of the spectrum reflect the two possible relaxation times of the system. Both of them get their minima value when $\kappa = 0$, $\lambda_{1(2)} = \lambda_{3(4)}$, and $\lambda_5 = \lambda_6 = \lambda_7 = \lambda_8$, giving rise to two second-order and a third-order LEPs, both of which have a square-root structure [25,35] (see Appendix A for the exact form of the eigensystem of Liouvillian $\mathcal{L}$). Note that, when $\kappa = 0$, $R_1 = R_3$, $R_2 = R_4$, and $R_5 = R_6 = R_7 \neq R_8$, which means that the corresponding eigenmatrix R_8 cannot coalesce with $R_{5,6,7}$. Therefore, λ_8 does not play a role in the $\kappa = 0$ LEP.

To investigate the physical connotations of the two types of LEPs, we reduce the master equation to the nonzero matrix elements of ρ:

$$\dot{\rho}_{bb} = i\frac{\Omega}{2}(\rho_{bc} - \rho_{cb}), \tag{8a}$$

$$\dot{\rho}_{cc} = -\gamma\rho_{cc} - i\frac{\Omega}{2}(\rho_{bc} - \rho_{cb}), \tag{8b}$$

$$\dot{\rho}_{bc} = -\gamma/2\rho_{bc} + i\frac{\Omega}{2}(\rho_{bb} - \rho_{cc}), \tag{8c}$$

$$\dot{\rho}_{aa} = \gamma\rho_{cc}. \tag{8d}$$

The coherent terms couple the populations ρ_{bb} and ρ_{cc} to the coherence ρ_{bc} and ρ_{cb} but have no contribution to the dynamics of coherence $\rho_{bc} + \rho_{cb}$ because $\dot{\rho}_{bc} + \dot{\rho}_{cb} = -\gamma/2(\rho_{bc} + \rho_{cb})$, which is only exponentially damped dynamics with decay rate $\gamma/2$. This means that we cannot characterize the LEP by observing the dynamics of $(\rho_{bc} + \rho_{cb})$. Meanwhile, as shown in Eq. (8a), the damping term, proportional to γ, does not affect ρ_{bb}. It contributes to the decay of ρ_{cc} and to the corresponding increase of ρ_{aa}. The competition between the coherent coupling and the dampling term of two states $\{|b\rangle, |c\rangle\}$ induces the third-order LEP (with the average decay rate $\gamma/2$), which is the phase transition point of the passive $\mathcal{PT}$ Hamiltonian [54]. Their contributions to $|a\rangle$ give rise to the second-order LEP (with average decay rate $\gamma/4$ and half-rotating frequency of the third-order LEP).

There are only three independent variables in Eqs. (8a)–(8d): $x = \rho_{bb}$, $y = \rho_{cc}$, and $z = -i(\rho_{bc} - \rho_{cb})$, which describe the dynamics of the subsystem $\{|b\rangle, |c\rangle\}$. With these new notations, we find the dynamics:

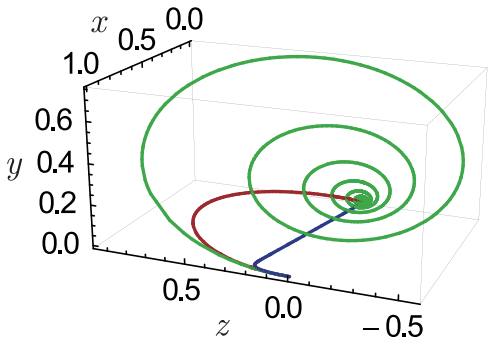

FIG. 3. The dynamics of x, y, z. Green line: oscillatory regime for $\gamma = 0.2\Omega$. Red line: Liouvillian exceptional point (LEP) for $\gamma = 2\Omega$. Blue line: overdamped regime for $\gamma = 10\Omega$.

$$\begin{pmatrix}\dot{x}\\ \dot{y}\\ \dot{z}\end{pmatrix} = \begin{pmatrix}0 & 0 & -\Omega/2\\ 0 & -\gamma & \Omega/2\\ \Omega & -\Omega & -\gamma/2\end{pmatrix}\begin{pmatrix}x\\ y\\ z\end{pmatrix}. \tag{9}$$

Eigenvalues of the 3×3 matrix in Eq. (10) are $-(\gamma \mp \kappa)/2$ $(= \lambda_{5,6})$ and $-\gamma/2$ $(= \lambda_7)$. The eigenvalues can be real or complex, leading to the two different regimes qualitatively analyzed above and inducing the the third-order LEP at $\kappa = 0$. In addition to that, we also derive their dynamical evolution analytically:

$$x(t) = \frac{\exp\left(-\frac{1}{2}\gamma t\right)}{\kappa^2}\left[(\gamma^2 - 2\Omega^2)\cosh\left(\frac{\kappa t}{2}\right) + \gamma\kappa\sinh\left(\frac{\kappa t}{2}\right) - 2\Omega^2\right], \tag{10a}$$

$$y(t) = \frac{\exp\left(-\frac{1}{2}\gamma t\right)}{\kappa^2}4\Omega^2\sinh^2\left(\frac{\kappa t}{4}\right), \tag{10b}$$

$$z(t) = \frac{\exp\left[-\frac{1}{2}(\gamma+\kappa)t\right]}{\kappa^2}\Omega\left\{\gamma\left[\exp\left(\frac{\kappa t}{2}\right) - 1\right]^2 + \kappa[\exp(\kappa t) - 1]\right\}. \tag{10c}$$

We show the dynamics of $x(t), y(t), z(t)$ in Fig. 3. When the decay rate is weak ($\gamma < 2\Omega$), the evolution is described by damped oscillation with decay rates $\gamma/2$ (subsystem) and $\gamma/4$ (full system), respectively. Obviously, increasing γ, the evolution approaching to the stationary state will become faster, which corresponds to the quantum anti-Zeno effect [61]. When the decay rate $\gamma > 2\Omega$, all the eigenvalues are real, and the dynamics exhibits an irreversible damping. In the limit of strong decay, $\gamma \gg 2\Omega$, the relaxation time scale is determined by

$$\frac{\gamma - \kappa}{2} \approx \frac{\Omega^2}{\gamma} \ll \gamma, \tag{11}$$

so that the system will experience the metastable process for a long time scale when the system appears stationary, before eventually relaxing to $\rho_{ss} = |a\rangle\langle a|$. This means that the larger γ is, the slower the system relaxes, which is a manifestation of the quantum Zeno [59,62–65]. Our results show that, for a dissipative system, quantum Zeno and anti-Zeno effects

correspond to the dynamical phenomena with strong and weak dissipation strengths, respectively. The LEP is thus the boundary between the quantum Zeno and anti-Zeno regimes and bridges the two previously independent effects [60,66].

The dynamics in the OD regime also leads to an effective decay from state $|b\rangle$ to state $|a\rangle$, with the effective decay rate:

$$\gamma_{b\to a} \approx \Omega^2/\gamma. \tag{12}$$

The same result can be found in Refs. [36,67] by employing perturbation theory and adiabatic elimination of states $|c\rangle$ for a weakly driven transition between $|b\rangle \leftrightarrow |c\rangle$. The above analysis shows that our dissipative three-level model can be used to engineer decay processes between states $|b\rangle$ and $|a\rangle$, like the Purcell effect in the spin-spring system with relaxation processes [68], just by tuning the Rabi frequency Ω.

C. Engineering the relaxation dynamics

1. Control Liouvillian dynamics through the initial state

As we discussed in last subsection, there exist two time scales of the relaxation process depending on the space spanned by the initial state. If the initial state is an arbitrary state in space $\{|a\rangle, \{|b\rangle, |c\rangle\}$, the relaxation time scale approaching to the stationary state $|a\rangle$ is determined by $\lambda_1 = -(\gamma-\kappa)/4$, and the fastest dynamical relaxation happens at the LEP ($\gamma = 2\Omega$) [see Fig. 4(a)]. On the other hand, if the initial state $\rho_{\rm in} \subseteq \{|b\rangle, |c\rangle\}$, as shown in Fig. 4(b), the relaxation time scale is determined by $\lambda_5 = -(\gamma-\kappa)/2$. This means that we can speed up relaxation in the convergence to stationarity by engineering the initial state, which is the so-called quantum Mpemba effect [1,2,22,69]. We can understand this by looking at the coefficients a_i of the initial state decomposing into the left eigenmatrices L_i. It can be shown that the coefficients of subspace $\{|b\rangle, |c\rangle\}$ decomposing into $L_{1\text{–}4}$ are all vanished, i.e., $a_{1\text{–}4} = {\rm Tr}[L_{1\sim4}\rho_{\rm in}] = 0$ (see Appendix A for further details). In this case,

$$\rho(t) = \rho_{ss} + \sum_{i=5}^{8} a_i \exp(\lambda_i t) R_i. \tag{13}$$

Therefore, the asymptotic decay rate is $-{\rm Re}[\lambda_5] = (\gamma-\kappa)/2$, which can get $g_{\rm LEP} = \gamma/2$. In Fig. 4(b), we compare the time scales for different initial states. It presents that, if the initial state is in the full space, the approach to the stationary state is governed by the eigenvalue λ_1 (red dashed line), while the initial state in the subspace leads to an exponentially faster relaxation to the stationary state with the rate given by $\lambda_5 = -(\gamma-\kappa)/2$ (green dashed line).

In addition to the dependence of the relaxation rate on the initial state, we also find that the observable values have significant effects on the relaxation rate [see Figs. 4(c) and 4(d)]. For instance, because ${\rm Tr}[|i\rangle\langle i|R_{1\text{–}4}] = 0 (i = a, b, c)$, the dynamics of the state populations approaching stationarity is governed by the eigenvalue λ_5 [Fig. 4(c)]. Moreover, the eigenmatrices $R_{5,6}$ describe the decay of $\sigma_{y,z}$ in the subspace $\{|b\rangle, |c\rangle\}$ with rates ${\rm Re}[\lambda_{5,6}] = (\gamma \mp \kappa)/2$, while $R_8(\lambda_8)$ is associated with σ_x (see Appendix A for further details). Whereas there occurs only damped dynamics in the subspace spanned by operators σ_x, the oscillatory evolution at frequency $|{\rm Im}[\lambda_5]|$ in the subspace spanned by vectors $\sigma_{y,z}$ allows us to identify the third-order LEP [28,31,70]. Considering that the final state $\rho_{ss} = |a\rangle\langle a|$ is independent of the parameters of the system, we can speed up the relaxation process by combining the acceleration effect of the LEP and the quantum Mpemba effect. Although the connection between these speedup effects will not be discussed in this paper, we note that they are not completely independent of each other, see the related studies in Ref. [23].

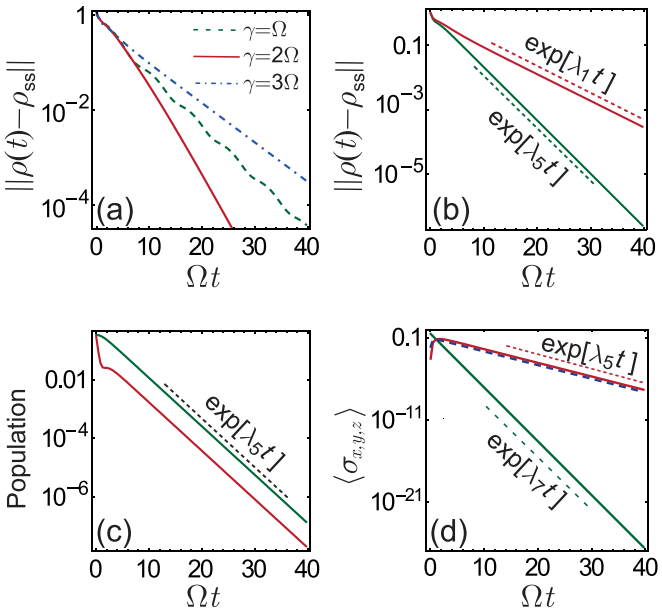

FIG. 4. (a) Distance between the time-evolved state $\rho(t)$ and the stationary state $\rho_{ss} = |a\rangle\langle a|$ for an initial random state in the full space with $\gamma = \Omega$ (dashed green line), $\gamma = 2\Omega$ (solid red line), and $\gamma = 3\Omega$ (dot-dashed blue line). In this original case, the approach to stationary is governed by the eigenvalue λ_1, and the Liouvillian exceptional point (LEP) leads to an exponentially faster convergence to the steady state with the rate $g_{\rm LEP} = \gamma/4 = \Omega/2$. (b) Distance between the time-evolved state $\rho(t)$ and the stationary state ρ_{ss}. We compare the case of an initial random state in the full space (red line) with the time evolution ensuing the initial state in the subspace of $\{|b\rangle, |c\rangle\}$ (green line). While in the original case the approach to stationary is governed by the eigenvalue λ_1(dashed red line), the special set of the initial state leads to an exponentially faster convergence to the steady state with the rate given by λ_5 (dashed green line). (c) Population dynamics vs evolution time for an initial random state in the full space (green line: ${\rm Tr}[\rho(t)|b\rangle\langle b|]$, red line: ${\rm Tr}[\rho(t)|c\rangle\langle c|]$), and the time scale is governed by the eigenvalue λ_5 (dashed line). (d) Observable dynamics vs evolution time for an initial random state in the full space (green line: $\langle\sigma_x\rangle = {\rm Tr}[\rho(t)\sigma_x]$, red line: $\langle\sigma_y\rangle = {\rm Tr}[\rho(t)\sigma_y]$, dashed blue line: $\langle\sigma_z\rangle = {\rm Tr}[\rho(t)\sigma_z]$, and the time scales are different: for σ_x, it is governed by the eigenvalue λ_7 (dashed green line), and for $\sigma_{y,z}$, they are governed by the eigenvalue λ_5 (dashed red line). All the y axes are in logarithmic scale, and the parameters for [(b)–(d)] are $\gamma/\Omega = 3$. We have to mention here that the real dynamics and exponential decay function do not coincide at short times. This is because, at short times, the decay rate is determined by all decay modes, while at long times, it decays with time exponentially.

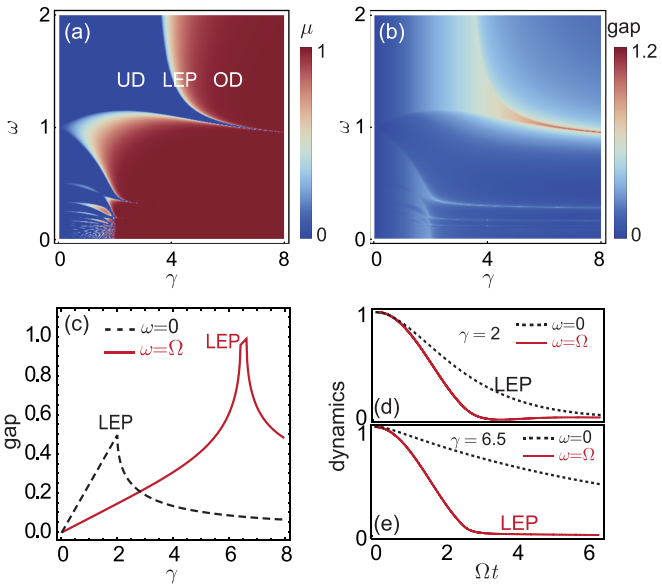

FIG. 5. (a) Phase diagram in the ω-γ plane. Color contour shows the dimensionless parameter μ. Here, we set $\Omega = 1, \tau = T/2.5$. Regions with $\mu = 0$ (the blue region) correspond to the underdamped (UD) regime, while $\mu \neq 0$ (the colored regions) correspond to the overdamped (OD) regime. These two regimes are bounded by the Liouvillian exceptional point (LEP). (b) Liouvillian spectral gap as function of ω and γ. (c) Liouvillian spectral gap as a function of γ with $\omega = 0$ (black dashed line), and $\omega = 1$ (red solid line), respectively. The dynamics of the population of $|b\rangle$ with $\omega = 0$ (dashed lines) and $\omega = \Omega$ (solid lines) for (c) $\omega = 2$ and (d) 6.5.

2. *Tuning the Liouvillian gap through Floquet modulation*

We find that the Liouvillian gap can be further increased under time-periodic (Floquet) dissipation with dissipation rate γ given by

$$\gamma(t) = \begin{cases} 0 & nT \leqslant t < nT + \tau, \\ \gamma & nT + \tau \leqslant t < (n+1)T. \end{cases} \tag{14}$$

Here, $n \in \mathbb{Z}$, $T = 2\pi/\omega$ is the period of the Liouvillian, i.e., $\mathcal{L}(t+T) = \mathcal{L}(t)$, with ω the modulation frequency, and τ is the off-duty time interval with no decay in each cycle. The density matrix at any time t is determined by the time-evolution operator $\mathcal{P}(t) = \mathbb{T}\exp(\int_0^t)\mathcal{L}(t')dt'$, where $\mathbb{T}$ is the time-ordering operator.

In analogy to the case of a non-Hermitian Hamiltonian system [64,71], we can now formally define a Floquet generator for our case, an effective time-independent generator $\mathcal{L}_F$ such that $\mathcal{P}(T) = \exp(\mathcal{L}_F T)$ [72–75]. Since the UD-OD transitions of the dynamics are determined by the degeneracies of the eigenvalues λ^P of the time-evolution operator $\mathcal{P}$, we adopt a dimensionless parameter $\mu = (|\lambda_+^P| - |\lambda_-^P|)/(|\lambda_+^P| + |\lambda_+^P|)$ to characterize the transition. Here, $\lambda_\pm^P$ denote two eigenvalues with bifurcation structure, and $\mu = 0$ marks the two eigenvalues are complex conjugate and the system is in the UD regime, while $\mu > 0$ are in the OD regime [see Fig. 5(a)]. We can see the Floquet method enriches the phase diagram. In contrast with the static dissipation ($\omega = 0$), where the phase transition and LEPs appear at $\Omega/\gamma = 2$, phase transitions under time-periodic dissipation depend on the modulation frequency ω and can occur at vanishing small dissipation strength.

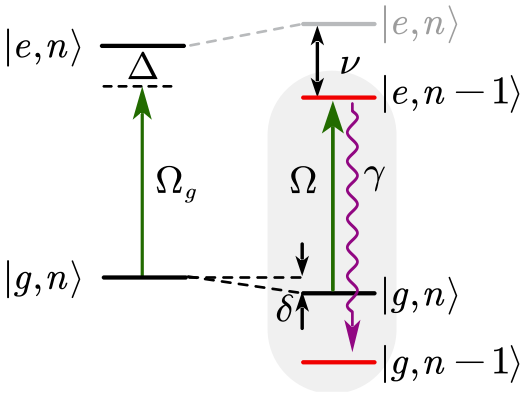

FIG. 6. Schematic of the sideband cooling process. The cooling laser with frequency ω_l drives the transition $|e\rangle \leftrightarrow |g\rangle$ with Rabi frequency Ω_g and detuning $\Delta = \omega_{eg} - \omega_l$, which leads to the ac Stark shift δ. Ω is the effective coupling strength between the red sideband transition $|g\rangle|n\rangle \leftrightarrow |e\rangle|n-1\rangle$, with n the phonon number and η the Lamb-Dicke parameter.

Beyond that, we are more interested in the effect of modulation on the energy gap. As shown in Figs. 5(b) and 5(c), the Floquet method increases the gap, and the maximal gap appears at the LEP, which is a different point with the static case. In the case of static dissipation ($\omega = 0$), $g_{\max} = g_{\text{LEP}} = \Omega/2$ when $\gamma/\Omega = 2$. The gap under time-periodic dissipation depends on the modulation frequency ω and can even be significantly increased to bigger than Ω [see Fig. 5(c)]. Figure 5(d) plots the dynamics of the population of state $|b\rangle$. We compare the two different cases, $\omega = 0$ (dashed lines) and $\omega = \Omega$ (the solid lines). These results illustrate that the LEP gap can surpass its static limit through Floquet engineering and thus further accelerate the relaxation.

IV. APPLICATIONS IN GROUND-STATE COOLING OF TRAPPED IONS

In the following, we demonstrate the power of this approach with a practical application, i.e., the ground-state cooling of trapped ions. Through analytical and numerical analysis, we illustrate that optimal cooling conditions in the sideband and EIT approaches can be obtained, which agree with existing experiments. Our LEP gap condition provides a perspective on optimal cooling conditions and may simulate more studies for a wide range of quantum engineering applications.

A. Sideband cooling

As shown in Fig. 6, we consider laser-ion interactions in the Lamb-Dicke limit. Dynamics is governed by the Hamiltonian:

$$H = \nu a^\dagger a + \Delta|e\rangle\langle e| - \tfrac{1}{2}\Omega_g\sigma^x + \tfrac{1}{2}\Omega(a^\dagger + a)\sigma^y, \tag{15}$$

and jump operator $J = \sqrt{\gamma}|g\rangle\langle e|$. Here, γ is the linewidth of the state $|e\rangle$, which is coupled to state $|g\rangle$ by a cooling laser field of frequency ω_l, Rabi frequency Ω_g, and detuning

$\Delta = \omega_{ge} - \omega_l$, where ω_{ge} is the frequency of the bare atomic transition $|e\rangle \leftrightarrow |g\rangle$. Also, ν is the trap frequency, and $a(a^\dagger)$ is the annihilation (creation) operator of phonons. Further, $\Omega = \eta\Omega_g$ describes the effective coupling between the phonon and internal state, and η is the Lamb-Dicke parameter. When $\Delta \simeq \nu$, the red sideband transition is nearly resonant, and the nonresonant transitions, i.e., the carrier transition and blue sideband transition, will induce the ac Stark shift to $|e\rangle(|g\rangle)$ by $\delta(-\delta)$, respectively. This is a good approximation that just considers the shift caused by the carrier transition, and under this approximation, we get $\delta = (\sqrt{\Omega_g^2 + \Delta^2} - \Delta)/2$.

To obtain the optimal cooling condition, we reduce the overall dynamics to a low-dimensional subsystem $\{|g\rangle|1\rangle, |g\rangle|0\rangle, |e\rangle|1\rangle, |e\rangle|0\rangle\}$ to obtain analytical results (see Appendix B for details). It is very helpful for us to understand the whole cooling process. Based on the perturbative calculations for this finite system, we get that $\lambda_{1(3)} = -(\gamma \mp \kappa')/4 + i(\Delta + 2\delta + \nu)/2$, and the gap:

$$g = \mathrm{Re}\left[\frac{1}{4}(\gamma - \kappa')\right], \tag{16}$$

with $\kappa' = \sqrt{[\gamma - 2i(\Delta + 2\delta - \nu)]^2 - 4\Omega^2}$. In Figs. 7(a)–7(d), we plot the analytical results of the spectra. It is obvious that the LEPs can only occur under the condition $\Delta + 2\delta - \nu = 0$. With $\delta = (\sqrt{\Omega_g^2 + \Delta^2} - \Delta)/2$, we obtain the condition to generate LEP:

$$\Omega^2 + \Delta^2 = \nu^2. \tag{17}$$

Under this condition, the eigenvalues $\lambda_{1(3)}$ become $\lambda_{1(3)} = -(\gamma \mp \kappa)/4 + i\nu$, whose real parts are the same as the three-level dissipative system shown in Fig. 2(b), and the imaginary parts connote rotating. In Ref. [10], authors use a pure numerical method of quantum control technique powered with automatic differentiation and obtain the same optimal cooling conditions. Here, we obtain the optimal conditions analytically in the context of LEPs. The physical mechanism underlying the condition in Eq. (17) is that the detuning Δ needs to be adjusted according to the ac Stark shift of the atomic levels to ensure that the red sideband transition is exactly on resonance. Under this premise, the level structure shown in Fig. 6 can be considered a simple three-level dissipative system, as discussed in Sec. III. When $\Omega \geqslant \gamma/2$, $\mathrm{Re}[\lambda_1] = \mathrm{Re}[\lambda_3] = -\gamma/4$, and we get the maximum value $g_{\max} = \gamma/4$. Particularly, when $\Omega = \gamma/2, \kappa = \sqrt{\gamma^2 - 4\Omega^2} = 0$, $\lambda_1 = \lambda_3$, and $R_1 = R_3$ (see Appendix B), the LEP occurs.

In Figs. 7(e) and 7(f), we compare the gap given by Eq. (16) (the solid lines) with the numerical results calculated from the full master equation (the dashed lines). Although our analytical results about spectrum and gap are obtained from the subsystem of the sideband cooling, they match very well with the numerical results calculated from the full system. As shown in Fig. 8, the real parts of the eigenvalues $\lambda_{i\geqslant 1}$, which give the relaxation rates of all the decay modes of the system, can mainly be divided into several characteristic intervals. It could be approximately $\{-\gamma/4, -\gamma/2, -3\gamma/4, -\gamma\}$ under the condition in Eq. (17) [see Figs. 8(a) and 8(b)]; otherwise, it becomes $\{0, -\gamma/2, -\gamma\}$ when $\Omega/\gamma > \frac{1}{2}$ [see Fig. 8(c)]. As shown in Figs. 8(c) and 8(d), different from the three-level dissipation system, it features a so-called metastable regime, either $\Omega/\gamma > \frac{1}{2}$ or $\Omega/\gamma < \frac{1}{2}$, which occurs when low-lying eigenvalues become separated from the rest of the spectrum [15]. The imaginary parts of the eigenvalues, which give the rotating rates of the decay modes approximately equal to $\mathrm{Im}[\lambda_{i\geqslant 1}] \approx (\Delta + 2\delta + n\nu)/2$ are mainly determined by phonon energy.

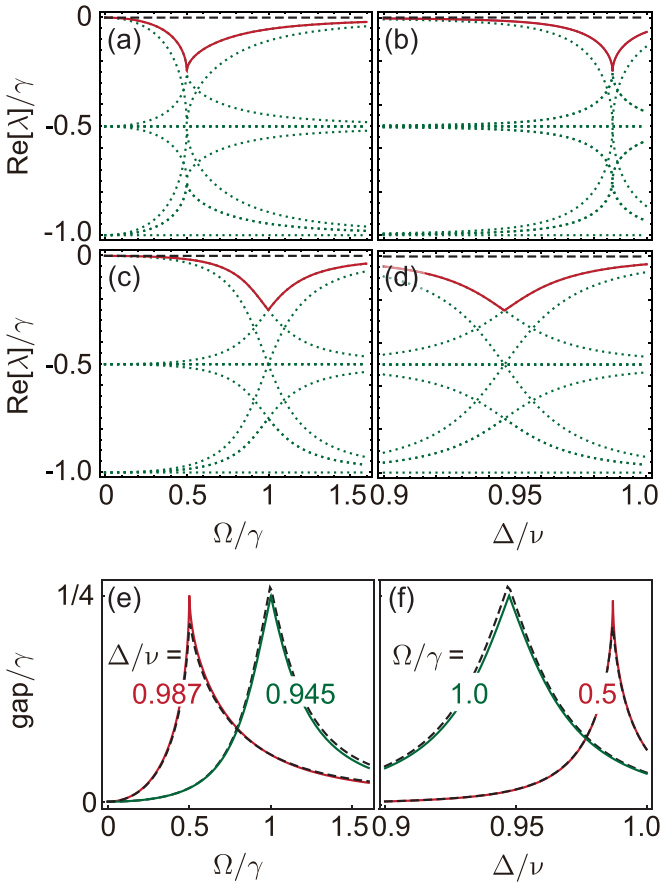

FIG. 7. Real parts of the Liouvillian spectra of the analytical results. The black dashed lines are λ_0, the red lines are $\mathrm{Re}[\lambda_1]$, and the green dotted lines are $\mathrm{Re}[\lambda_{i>1}]$. The parameters are (a) $\Delta = 0.987\nu$, (b) $\Omega = 0.5\gamma$, (c) $\Delta = 0.945\nu$, and (d) $\Omega = \gamma$. Gap as functions of (e) Ω/γ and (f) Δ/ν. (e) $\Delta = 0.987\nu$ (red solid line) and $= 0.945\nu$ (green solid line), (f) $\Omega = \Omega_g\eta = 0.5\gamma$ (red solid line) and $= \gamma$ (blue solid line), respectively. The solid lines correspond to the analytical results from Eq. (16), and the black dashed lines are the results from the full Liouvillian. The other parameters are $\eta = 0.1$, $\nu = 1$, and $\gamma = 0.032$.

In Fig. 9(a), we plot the gap g as functions of Ω/γ and Δ/ν by using the full master equation. Point A corresponds to the LEP, and the dashed white line is the condition of $g = g_{\max}$ that combines the red sideband transition resonant condition in Eq. (17), as we discussed before. The numerical results and the analytical results are matched very well. Figure 9(b) shows the dynamics of the full system for some set of parameters [points A–D in Fig. 9(a)]. It indicates that the gap g provides a good description of the cooling time. At the LEP, the system not only reaches stationary state at a significantly faster pace but also obtains a lower phonon number [see Figs. 9(c) and

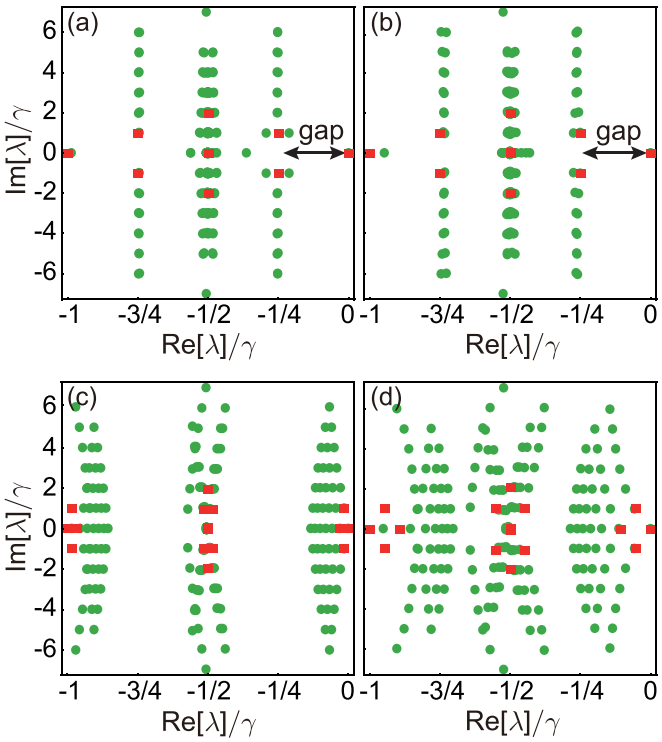

FIG. 8. Spectral properties of the Liouvillian. In the Liouvillian exceptional point (LEP) condition ($\Omega^2 + \Delta = \nu^2$), the parameters of $(\Omega/\gamma, \Delta/\nu)$ are (a) (0.5, 0.987), (b) (1, 0.945). Not in the LEP condition ($\Omega^2 + \Delta \neq \nu^2$), the parameters of $(\Omega/\gamma, \Delta/\nu)$ are (c) (1, 0.987), and (d) (0.2, 1). The green dots are the results from the full Liouvillian, and the red squares are the eigenvalues of the analytical results. The other parameters are the same as in Fig. 7.

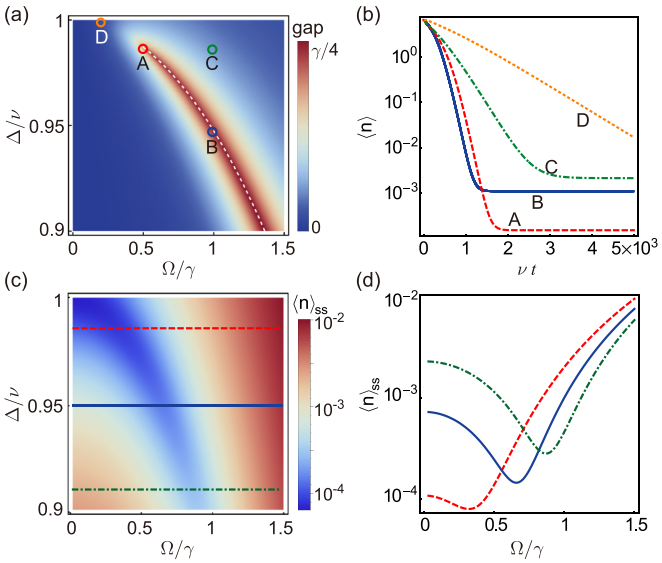

FIG. 9. (a) Gap properties of the full Liouvillian. The white dashed line corresponds to $\Omega^2 + \Delta^2 = \nu^2$. The parameters $(\Omega/\gamma, \Delta/\nu)$ are (A) (0.5, 0.987), (B) (1, 0.945), (C) (1, 0.987), and (D) (0.2, 1) and $g_A = g_B > g_C > g_D$. (b) The average phonon number $\langle n \rangle$ as a function of time calculated with the full master equation with the parameters of A–D, respectively. (c) Cooling limit $\langle n \rangle_{ss}$ as functions of detuning Δ/ν and effective Rabi frequency of red sideband transition Ω/γ. (d) $\langle n \rangle_{ss}$ as a function of effective Rabi frequency of red sideband transition Ω/γ, with $\Delta/\nu = 0.987$ (red dashed line), 0.95 (blue solid line), and 0.91 (green dot-dashed line). The other parameters are the same as in Fig. 7.

9(d)]. Therefore, we believe that the best cooling effect can be obtained by the system parameters at the LEP.

B. EIT cooling

For the EIT cooling method discussed in Refs. [5,7,9], we find that the optimal parameter selection could be explained by the gap at the LEP. As shown in Fig. 10(a), the detuned laser of frequency ω_r and Rabi frequency Ω_r couples the transition $|r\rangle \leftrightarrow |e\rangle$ with detuning $\Delta_r = \omega_r - \omega_{er}$. It leads to two dressed states $|+\rangle$ and $|-\rangle$ shown in Fig. 10(b) with energy $\omega_+ = \Delta_r + \delta_r$, $\omega_- = -\delta_r$ [5,76], respectively. Here, $\delta_r = (\sqrt{\Omega_r^2 + \Delta_r^2} - |\Delta_r|)/2$ is the ac Stark shift induced by the coupling laser Ω_r.

If we turn to the detuning frequency Δ_g of Ω_g close to Δ_r, then $|+\rangle = \sin\phi|e\rangle + \cos\phi|r\rangle$ $(\tan\phi = \Omega_r/[\sqrt{\Omega_r^2 + \Delta_r^2} + \Delta_r)]$ is chosen to replace $|e\rangle$ in the sideband cooling model [see Fig. 10(c)]. Here, we just replace

$$\gamma \to \gamma_+ = \gamma_e \sin^2\phi = \frac{\gamma_e}{2}\left(1 - \frac{\Delta_r}{\sqrt{\Omega_r^2 + \Delta_r^2}}\right), \tag{18}$$

$$\Omega \to \eta \sin\phi \Omega_g, \tag{19}$$

$$\Delta \to \omega_+ - \Delta_g. \tag{20}$$

Then the optimal condition of $g_{\max}$ shown in Eq. (17) becomes

$$\frac{\eta^2}{2}\left(1 - \frac{\Delta_r}{\sqrt{\Omega_r^2 + \Delta_r^2}}\right)\Omega_g^2 + \left(\frac{\sqrt{\Omega_r^2 + \Delta_r^2} + \Delta_r}{2} - \Delta_g\right)^2 = \nu^2. \tag{21}$$

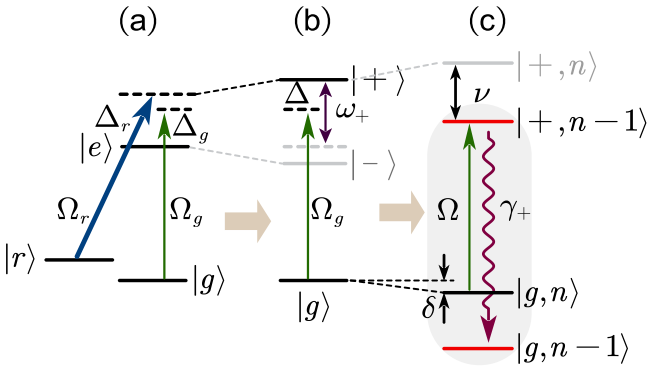

FIG. 10. (a) Levels and transitions of the electromagnetically induced transparency (EIT) cooling scheme (found in many species used for ion trapping). (b) The dressed levels that the cooling laser Ω_g couples. (c) When the cooling laser is near resonant with the red sideband transition of the dressed state $|+\rangle$, this EIT cooling model can be equivalent to the model we discussed in Sec. IV A.

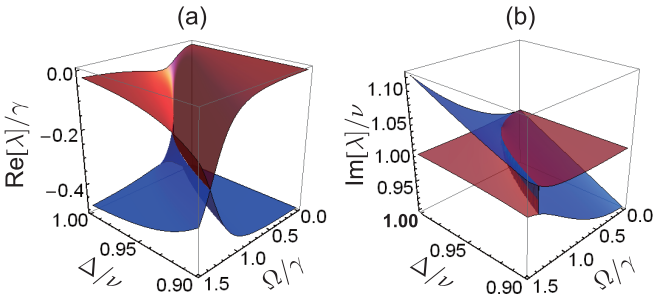

FIG. 11. (a) Real and (b) imaginary parts of λ_2 (red) and λ_4 (blue).

If we ignore the higher-order terms $O(\eta^2)$, Eq. (22) can be rewritten as

$$\frac{\sqrt{\Omega_r^2+\Delta_r^2}+\Delta_r}{2}-\Delta_g=\delta_r+\Delta_r-\Delta_g=\nu. \tag{22}$$

It is in accordance with the generalized cooling condition given in the experimental works of Ref. [7,9]; thus, our LEP method offers a fresh understanding of optical cooling condition.

V. DISCUSSION

In summary, we have studied how to engineer relaxation dynamics of Markovian open quantum systems with an arbitrary initial state. Our results have shown, for an arbitrary initial state, a speedup relaxation can be achieved by setting the parameters of the system at LEP, where the slowest decay mode degenerates with a faster decay mode. In addition, our LEP-based accelerated approach can be applied to accelerate the relaxation in Floquet dissipative quantum dynamics. We have shown the relaxation processes can be dramatically faster than the static case by periodically modulating the dissipation strength. Finally, we have demonstrated the applications of our method for speeding up cooling processes in ground-state cooling of trapped ions. In a broader view, our ideas may still be instructive for optimal parameter options to accelerate the cooling process even for simultaneous cooling of multiple phonon modes in a ion crystal. Therefore, our method is general and would facilitate the optical parameter settings in the experiments with open quantum many-body systems. Together with well-developed techniques of engineering quantum states, in this paper, we provide a powerful tool for exploring and utilizing true quantum LEP effects as examples of engineered relaxation dynamics [69].

ACKNOWLEDGMENTS

This paper was supported by the Natural Science Foundation of Hunan Province of China (Grants No. 2023JJ30626, No. 2022RC1194, and No. 2023JJ10052) and the National Nature Science Foundation of China (Grants No. 12174448, No. 12074433, and No. 12004430).

APPENDIX A: LIOUVILLIAN SPECTRUM OF A DISSIPATIVE THREE-LEVEL SYSTEM

We consider a simple dissipative three-level system of Fig. 2(b), and the dynamics is described by a Lindblad master equation:

$$\mathcal{L}\rho=-i[H,\rho]+J\rho J^\dagger-\tfrac{1}{2}\{J^\dagger J,\rho\}, \tag{A1}$$

with the Hamiltonian $H=\Omega/2(|c\rangle\langle b|+|b\rangle\langle c|)$ and a jump operator $J=\sqrt{\gamma}|a\rangle\langle c|$.

To study the Liouvilian spectra and LEPs, we first represent the Liouvillian superoperator $\mathcal{L}$ in a matrix form by recasting the above master equation as a matrix differential equation for the vectorized state of the density operator ρ. With the definitions that $|a\rangle=(1,0,0)^T$, $|b\rangle=(0,1,0)^T$, and $|c\rangle=(0,0,1)^T$, the Liouvillian superoperator is given by

$$\mathcal{L}=\begin{pmatrix}
0 & 0 & 0 & 0 & 0 & 0 & 0 & 0 & \gamma\\
0 & 0 & \frac{i\Omega}{2} & 0 & 0 & 0 & 0 & 0 & 0\\
0 & \frac{i\Omega}{2} & -\frac{\gamma}{2} & 0 & 0 & 0 & 0 & 0 & 0\\
0 & 0 & 0 & 0 & 0 & 0 & -\frac{i\Omega}{2} & 0 & 0\\
0 & 0 & 0 & 0 & 0 & \frac{i\Omega}{2} & 0 & -\frac{i\Omega}{2} & 0\\
0 & 0 & 0 & 0 & \frac{i\Omega}{2} & -\frac{\gamma}{2} & 0 & 0 & -\frac{i\Omega}{2}\\
0 & 0 & 0 & -\frac{i\Omega}{2} & 0 & 0 & -\frac{\gamma}{2} & 0 & 0\\
0 & 0 & 0 & 0 & -\frac{i\Omega}{2} & 0 & 0 & -\frac{\gamma}{2} & \frac{i\Omega}{2}\\
0 & 0 & 0 & 0 & 0 & -\frac{i\Omega}{2} & 0 & \frac{i\Omega}{2} & -\gamma
\end{pmatrix}. \tag{A2}$$

The eigenvalues of $\mathcal{L}$ are

$$\lambda_0=0,\quad \lambda_{1(2)}=-\frac{1}{4}(\gamma-\kappa),\quad \lambda_{3(4)}=-\frac{1}{4}(\gamma+\kappa),\quad \lambda_{5,6}=-\frac{1}{2}(\gamma\mp\kappa),\quad \lambda_{7(8)}=-\frac{\gamma}{2}, \tag{A3}$$

with $\kappa=\sqrt{\gamma^2-4\Omega^2}$. Both the right and left eigenmatrices of the Liouvillian superoperators can be constructed to be Hermitian; they are

$$R_0=\rho_{ss}=\begin{pmatrix}1&0&0\\0&0&0\\0&0&0\end{pmatrix},\quad R_1\ \propto\begin{pmatrix}0&-\frac{i(\gamma+\kappa)}{2\Omega}&1\\\frac{i(\gamma+\kappa)}{2\Omega}&0&0\\1&0&0\end{pmatrix},\quad R_2\ \propto\begin{pmatrix}0&\frac{(\gamma+\kappa)}{2\Omega}&i\\\frac{(\gamma+\kappa)}{2\Omega}&0&0\\-i&0&0\end{pmatrix},$$

$$R_3 \propto \begin{pmatrix} 0 & -\frac{i(\gamma-\kappa)}{2\Omega} & 1 \\ \frac{i(\gamma-\kappa)}{2\Omega} & 0 & 0 \\ 1 & 0 & 0 \end{pmatrix}, \quad R_4 \propto \begin{pmatrix} 0 & \frac{(\gamma-\kappa)}{2\Omega} & i \\ \frac{(\gamma-\kappa)}{2\Omega} & 0 & 0 \\ -i & 0 & 0 \end{pmatrix}, \quad R_5 \propto \begin{pmatrix} -\frac{2\gamma}{\gamma-\kappa} & 0 & 0 \\ 0 & \frac{2\gamma}{\gamma-\kappa}-1 & \frac{i(\gamma+\kappa)}{2\Omega} \\ 0 & -\frac{i(\gamma+\kappa)}{2\Omega} & 1 \end{pmatrix},$$

$$R_6 \propto \begin{pmatrix} -\frac{2\gamma}{\gamma+\kappa} & 0 & 0 \\ 0 & \frac{2\gamma}{\gamma+\kappa}-1 & \frac{i(\gamma-\kappa)}{2\Omega} \\ 0 & -\frac{i(\gamma-\kappa)}{2\Omega} & 1 \end{pmatrix}, \quad R_7 \propto \begin{pmatrix} -2 & 0 & 0 \\ 0 & 1 & \frac{i\gamma}{2\Omega} \\ 0 & -\frac{i\gamma}{2\Omega} & 1 \end{pmatrix}, \quad R_8 \propto \begin{pmatrix} 0 & 0 & 0 \\ 0 & 0 & 1 \\ 0 & 1 & 0 \end{pmatrix}, \tag{A4}$$

$$L_0 = \begin{pmatrix} 1 & 0 & 0 \\ 0 & 1 & 0 \\ 0 & 0 & 1 \end{pmatrix}, \quad L_1 \propto \begin{pmatrix} 0 & \frac{i(\gamma+\kappa)}{2\Omega} & 1 \\ -\frac{i(\gamma+\kappa)}{2\Omega} & 0 & 0 \\ 1 & 0 & 0 \end{pmatrix}, \quad L_2 \propto \begin{pmatrix} 0 & \frac{(\gamma+\kappa)}{2\Omega} & -i \\ \frac{(\gamma+\kappa)}{2\Omega} & 0 & 0 \\ i & 0 & 0 \end{pmatrix},$$

$$L_3 \propto \begin{pmatrix} 0 & \frac{i(\gamma-\kappa)}{2\Omega} & 1 \\ -\frac{i(\gamma-\kappa)}{2\Omega} & 0 & 0 \\ 1 & 0 & 0 \end{pmatrix}, \quad L_4 \propto \begin{pmatrix} 0 & \frac{(\gamma-\kappa)}{2\Omega} & -i \\ \frac{(\gamma-\kappa)}{2\Omega} & 0 & 0 \\ i & 0 & 0 \end{pmatrix}, \quad L_5 \propto \begin{pmatrix} 0 & 0 & 0 \\ 0 & \frac{2\gamma}{\gamma-\kappa}-1 & -\frac{i(\gamma+\kappa)}{2\Omega} \\ 0 & \frac{i(\gamma+\kappa)}{2\Omega} & 1 \end{pmatrix},$$

$$L_6 \propto \begin{pmatrix} 0 & 0 & 0 \\ 0 & \frac{2\gamma}{\gamma+\kappa}-1 & -\frac{i(\gamma-\kappa)}{2\Omega} \\ 0 & \frac{i(\gamma-\kappa)}{2\Omega} & 1 \end{pmatrix}, \quad L_7 \propto \begin{pmatrix} 0 & 0 & 0 \\ 0 & 1 & -\frac{i\gamma}{2\Omega} \\ 0 & \frac{i\gamma}{2\Omega} & 1 \end{pmatrix}, \quad L_8 \propto \begin{pmatrix} 0 & 0 & 0 \\ 0 & 0 & 1 \\ 0 & 1 & 0 \end{pmatrix}. \tag{A5}$$

If the initial state is in this subspace $\{|b\rangle, |c\rangle\}$, it is easily get that $a_{1\text{–}4} = \mathrm{Tr}[L_{1\text{–}4}\rho_{\mathrm{in}}] = 0$. It means that the coefficients of subspace $\{|b\rangle, |c\rangle\}$ decomposing into $L_{1\text{–}4}$ are all vanished.

APPENDIX B: LIOUVILLIAN SPECTRUM OF THE SUBSYSTEM OF GROUND-STATE COOLING PROCESS

For the subsystem $\{|e\rangle|1\rangle, |e\rangle|0\rangle, |g\rangle|1\rangle, |g\rangle|0\rangle\}$, we calculate the spectrum of its superoperator $\mathcal{L}$ and get

$$\lambda_0 = 0, \quad \lambda_1 = \lambda_2^* = -\frac{\gamma-\kappa'}{4} + i\frac{\alpha}{2},$$
$$\lambda_3 = \lambda_4^* = -\frac{\gamma+\kappa'}{4} + i\frac{\alpha}{2},$$
$$\lambda_5 = \lambda_6^* = -\frac{\gamma}{2} + i\alpha, \quad \lambda_{7(8)} = -\frac{2\gamma \mp \epsilon}{4},$$
$$\lambda_{9(10)} = -\frac{2\gamma \mp \epsilon'}{4},$$
$$\lambda_{11} = \lambda_{12}^* = -\frac{3\gamma-\kappa'}{4} - i\frac{\alpha}{2},$$
$$\lambda_{13} = \lambda_{14}^* = -\frac{3\gamma+\kappa'}{4} - i\frac{\alpha}{2}, \ \lambda_{15} = -\gamma, \tag{B1}$$

with

$$\kappa' = \sqrt{(\gamma+2i\beta)^2 - 4\Omega^2}, \tag{B2}$$

$$\alpha = \Delta + 2\delta + \nu, \tag{B3}$$

$$\epsilon = \sqrt{-2\sqrt{(4(\beta^2+\Omega^2)+\gamma^2)^2 - 16\gamma^2\Omega^2} - 8\beta^2 + 2\gamma^2 - 8\Omega^2}, \tag{B4}$$

$$\epsilon' = \sqrt{2\sqrt{(4(\beta^2+\Omega^2)+\gamma^2)^2 - 16\gamma^2\Omega^2} - 8\beta^2 + 2\gamma^2 - 8\Omega^2}, \tag{B5}$$

where $\beta = 2\delta + \Delta - \nu$. The corresponding eigenmatrices are

$$R_0 = \begin{pmatrix} 0 & 0 & 0 & 0 \\ 0 & 0 & 0 & 0 \\ 0 & 0 & 0 & 0 \\ 0 & 0 & 0 & 1 \end{pmatrix}, \quad R_1 \propto \begin{pmatrix} 0 & 0 & 0 & 0 \\ 0 & 0 & 0 & \frac{2\Omega}{2i\beta+\gamma+\kappa'^*} \\ 0 & 0 & 0 & 1 \\ 0 & \frac{2\Omega}{-2i\beta+\gamma+\kappa'} & 1 & 0 \end{pmatrix}, \quad R_2 \propto \begin{pmatrix} 0 & 0 & 0 & 0 \\ 0 & 0 & 0 & -\frac{2i\Omega}{2i\beta+\gamma+\kappa'^*} \\ 0 & 0 & 0 & -i \\ 0 & \frac{2i\Omega}{-2i\beta+\gamma+\kappa'} & i & 0 \end{pmatrix},$$

$$R_3 \propto \begin{pmatrix} 0 & 0 & 0 & 0 \\ 0 & 0 & 0 & -\frac{2\Omega}{-2i\beta-\gamma+\kappa'^*} \\ 0 & 0 & 0 & 1 \\ 0 & -\frac{2\Omega}{2i\beta-\gamma+\kappa'} & 1 & 0 \end{pmatrix}, \quad R_4 \propto \begin{pmatrix} 0 & 0 & 0 & 0 \\ 0 & 0 & 0 & \frac{2i\Omega}{-2i\beta-\gamma+\kappa'^*} \\ 0 & 0 & 0 & -i \\ 0 & -\frac{2i\Omega}{2i\beta-\gamma+\kappa'} & i & 0 \end{pmatrix},$$

$$R_5 \propto \begin{pmatrix} 0 & 0 & 0 & 1 \\ 0 & 0 & 0 & 0 \\ 0 & 0 & 0 & 0 \\ 1 & 0 & 0 & 0 \end{pmatrix}, \quad R_6 \propto \begin{pmatrix} 0 & 0 & 0 & -i \\ 0 & 0 & 0 & 0 \\ 0 & 0 & 0 & 0 \\ i & 0 & 0 & 0 \end{pmatrix}, \quad R_7 \propto \begin{pmatrix} 0 & 0 & 0 & 0 \\ 0 & -\frac{2\gamma-\epsilon}{4\gamma} & -\frac{\epsilon\Omega}{\gamma(4i\beta+\epsilon)} & 0 \\ 0 & -\frac{\epsilon\Omega}{\gamma(\epsilon-4i\beta)} & -\frac{2\gamma+\epsilon}{4\gamma} & 0 \\ 0 & 0 & 0 & 1 \end{pmatrix},$$

$$R_8 \propto \begin{pmatrix} 0 & 0 & 0 & 0 \\ 0 & -\frac{2\gamma+\epsilon}{4\gamma} & \frac{\epsilon\Omega}{\gamma(4i\beta-\epsilon)} & 0 \\ 0 & \frac{\epsilon\Omega}{\gamma(-4i\beta-\epsilon)} & -\frac{2\gamma-\epsilon}{4\gamma} & 0 \\ 0 & 0 & 0 & 1 \end{pmatrix}, \quad R_9 \propto \begin{pmatrix} 0 & 0 & 0 & 0 \\ 0 & -\frac{2\gamma-\epsilon'}{4\gamma} & -\frac{\epsilon'\Omega}{\gamma(4i\beta+\epsilon')} & 0 \\ 0 & -\frac{\epsilon'\Omega}{\gamma(\epsilon'-4i\beta)} & -\frac{2\gamma+\epsilon'}{4\gamma} & 0 \\ 0 & 0 & 0 & 1 \end{pmatrix}, \quad R_{10} \propto \begin{pmatrix} 0 & 0 & 0 & 0 \\ 0 & -\frac{2\gamma+\epsilon'}{4\gamma} & \frac{\epsilon'\Omega}{\gamma(-\epsilon'+4i\beta)} & 0 \\ 0 & \frac{\epsilon'\Omega}{\gamma(-\epsilon'-4i\beta)} & -\frac{2\gamma-\epsilon'}{4\gamma} & 0 \\ 0 & 0 & 0 & 1 \end{pmatrix},$$

$$R_{11} \propto \begin{pmatrix} 0 & -1 & -\frac{-2i\beta+\gamma+\kappa'}{2\Omega} & 0 \\ -1 & 0 & 0 & \frac{2\Omega}{2i\beta-\gamma+\kappa'} \\ -\frac{2i\beta+\gamma+\kappa'^*}{2\eta\Omega_g} & 0 & 0 & 1 \\ 0 & \frac{2\Omega}{-2i\beta-\gamma+\kappa'^*} & 1 & 0 \end{pmatrix},$$

$$R_{12} \propto \begin{pmatrix} 0 & -i & -\frac{i(-2i\beta+\gamma+\kappa')}{2\Omega} & 0 \\ i & 0 & 0 & \frac{2i\Omega}{2i\beta-\gamma+\kappa'} \\ \frac{i(2i\beta+\gamma+\kappa'^*)}{2\Omega} & 0 & 0 & i \\ 0 & -\frac{2i\Omega}{-2i\beta-\gamma+\kappa'^*} & -i & 0 \end{pmatrix},$$

$$R_{13} \propto \begin{pmatrix} 0 & -1 & -\frac{-2i\beta+\gamma-\kappa'}{2\Omega} & 0 \\ -1 & 0 & 0 & \frac{2\Omega}{2i\beta-\gamma-\kappa'} \\ -\frac{2i\beta+\gamma-\kappa'^*}{2\eta\Omega_g} & 0 & 0 & 1 \\ 0 & \frac{2\Omega}{-2i\beta-\gamma-\kappa'^*} & 1 & 0 \end{pmatrix},$$

$$R_{14} \propto \begin{pmatrix} 0 & -i & -\frac{i(-2i\beta+\gamma-\kappa')}{2\Omega} & 0 \\ i & 0 & 0 & \frac{2i\Omega}{2i\beta-\gamma-\kappa'} \\ \frac{i(2i\beta+\gamma-\kappa'^*)}{2\Omega} & 0 & 0 & i \\ 0 & -\frac{2i\Omega}{-2i\beta-\gamma-\kappa'^*} & -i & 0 \end{pmatrix}, \quad R_{15} \propto \begin{pmatrix} 1 & 0 & 0 & 0 \\ 0 & -1 & 0 & 0 \\ 0 & 0 & -1 & 0 \\ 0 & 0 & 0 & 1 \end{pmatrix}.$$

We are interested in the low-lying eigenvalues, especially λ_1 which determines the spectral gap $g = \frac{1}{4}(\gamma - \kappa')$. We can see that, when $\beta = 2\delta + \Delta - \nu = 0$ and $\gamma = 2\Omega$, we get $\kappa' = 0$ and $\lambda_{1(2)} = \lambda_{3(4)}$, $\lambda_{11(12)} = \lambda_{13(14)}$ (see Fig. 11). As a result, we can find sets of simultaneous second-order LEPs.

[1] F. Carollo, A. Lasanta, and I. Lesanovsky, Exponentially accelerated approach to stationarity in Markovian open quantum systems through the Mpemba effect, Phys. Rev. Lett. **127**, 060401 (2021).

[2] S. Kochsiek, F. Carollo, and I. Lesanovsky, Accelerating the approach of dissipative quantum spin systems towards stationarity through global spin rotations, Phys. Rev. A **106**, 012207 (2022).

[3] T. Van Vu and Y. Hasegawa, Toward relaxation asymmetry: Heating is faster than cooling, Phys. Rev. Res. **3**, 043160 (2021).

[4] A. Lapolla and A. Godec, Faster uphill relaxation in thermodynamically equidistant temperature quenches, Phys. Rev. Lett. **125**, 110602 (2020).

[5] G. Morigi, J. Eschner, and C. H. Keitel, Ground state laser cooling using electromagnetically induced transparency, Phys. Rev. Lett. **85**, 4458 (2000).

[6] L. Feng, W. L. Tan, A. De, A. Menon, A. Chu, G. Pagano, and C. Monroe, Efficient ground-state cooling of large trapped-ion chains with an electromagnetically-induced-transparency tripod scheme, Phys. Rev. Lett. **125**, 053001 (2020).

[7] M. Qiao, Y. Wang, Z. Cai, B. Du, P. Wang, C. Luan, W. Chen, H.-R. Noh, and K. Kim, Double-electromagnetically-induced-transparency ground-state cooling of stationary two-dimensional ion crystals, Phys. Rev. Lett. **126**, 023604 (2021).

[8] S. Zhang, J.-Q. Zhang, W. Wu, W.-S. Bao, and C. Guo, Fast cooling of trapped ion in strong sideband coupling regime, New J. Phys. **23**, 023018 (2021).

[9] J. Zhang, M.-C. Zhang, Y. Xie, C.-W. Wu, B.-Q. Ou, T. Chen, W.-S. Bao, P. Haljan, W. Wu, S. Zhang *et al.*, Parallel electromagnetically induced transparency near ground-state cooling of a trapped-ion crystal, Phys. Rev. Appl. **18**, 014022 (2022).

[10] X.-Q. Li, S. Zhang, J. Zhang, W. Wu, C. Guo, and P.-X. Chen, Fast laser cooling using optimal quantum control Xie-Qian, Phys. Rev. A **104**, 043106 (2021).

[11] J. Honer, R. Löw, H. Weimer, T. Pfau, and H. P. Büchler, Artificial atoms can do more than atoms: Deterministic single photon subtraction from arbitrary light fields, Phys. Rev. Lett. **107**, 093601 (2011).

[12] C. Tresp, C. Zimmer, I. Mirgorodskiy, H. Gorniaczyk, A. Paris-Mandoki, and S. Hofferberth, Single-photon absorber based on strongly interacting Rydberg atoms, Phys. Rev. Lett. **117**, 223001 (2016).

[13] A. Paris-Mandoki, C. Braun, J. Kumlin, C. Tresp, I. Mirgorodskiy, F. Christaller, H. P. Büchler, and S. Hofferberth, Free-space quantum electrodynamics with a single Rydberg superatom, Phys. Rev. X **7**, 041010 (2017).

[14] N. Stiesdal, H. Busche, J. Kumlin, K. Kleinbeck, H. P. Büchler, and S. Hofferberth, Observation of collective decay dynamics of a single Rydberg superatom, Phys. Rev. Res. **2**, 043339 (2020).

[15] K. Macieszczak, M. Guţă, I. Lesanovsky, and J. P. Garrahan, Towards a theory of metastability in open quantum dynamics, Phys. Rev. Lett. **116**, 240404 (2016).

[16] M. Žnidarič, Relaxation times of dissipative many-body quantum systems, Phys. Rev. E **92**, 042143 (2015).

[17] T. Haga, M. Nakagawa, R. Hamazaki, and M. Ueda, Liouvillian skin effect: Slowing down of relaxation processes without gap closing, Phys. Rev. Lett. **127**, 070402 (2021).

[18] E. B. Mpemba and D. G. Osborne, Cool? Phys. Educ. **4**, 172 (1969).

[19] Z. Lu and O. Raz, Nonequilibrium thermodynamics of the Markovian Mpemba effect and its inverse, Proc. Natl. Acad. Sci. USA **114**, 5083 (2017).

[20] I. Klich, O. Raz, O. Hirschberg, and M. Vucelja, Mpemba index and anomalous relaxation, Phys. Rev. X **9**, 021060 (2019).

[21] A. Kumar and J. Bechhoefer, Exponentially faster cooling in a colloidal system, Nature (London) **584**, 64 (2020).

[22] A. K. Chatterjee, S. Takada, and H. Hayakawa, Quantum Mpemba effect in a quantum dot with reservoirs, Phys. Rev. Lett. **131**, 080402 (2023).

[23] G. Teza, R. Yaacoby, and O. Raz, Eigenvalue crossing as a phase transition in relaxation dynamics, Phys. Rev. Lett. **130**, 207103 (2023).

[24] I. I. Arkhipov, A. Miranowicz, F. Minganti, and F. Nori, Liouvillian exceptional points of any order in dissipative linear bosonic systems: Coherence functions and switching between $\mathcal{PT}$ and anti-$\mathcal{PT}$ symmetries, Phys. Rev. A **102**, 033715 (2020).

[25] W. D. Heiss, The physics of exceptional points, J. Phys. A: Math. Theor. **45**, 444016 (2012).

[26] F. Minganti, A. Miranowicz, R. W. Chhajlany, and F. Nori, Quantum exceptional points of non-Hermitian Hamiltonians and Liouvillians: The effects of quantum jumps, Phys. Rev. A **100**, 062131 (2019).

[27] W. Chen, M. Abbasi, Y. N. Joglekar, and K. W. Murch, Quantum jumps in the non-Hermitian dynamics of a superconducting qubit, Phys. Rev. Lett. **127**, 140504 (2021).

[28] W. Chen, M. Abbasi, B. Ha, S. Erdamar, Y. N. Joglekar, and K. W. Murch, Decoherence induced exceptional points in a dissipative superconducting qubit, Phys. Rev. Lett. **128**, 110402 (2022).

[29] P. Kumar, K. Snizhko, Y. Gefen, and B. Rosenow, Optimized steering: Quantum state engineering and exceptional points, Phys. Rev. A **105**, L010203 (2022).

[30] W. Nie, M. Antezza, Y. X. Liu, and F. Nori, Dissipative topological phase transition with strong system-environment coupling, Phys. Rev. Lett. **127**, 250402 (2021).

[31] F. Minganti, A. Biella, N. Bartolo, and C. Ciuti, Spectral theory of Liouvillians for dissipative phase transitions, Phys. Rev. A **98**, 042118 (2018).

[32] Á. Rubio-García, Á. L. Corps, A. Relaño, R. A. Molina, F. Pérez-Bernal, J. E. García-Ramos, and J. Dukelsky, Exceptional spectral phase in a dissipative collective spin model, Phys. Rev. A **106**, L010201 (2022).

[33] S. Longhi, Unraveling the non-Hermitian skin effect in dissipative systems, Phys. Rev. B **102**, 201103(R) (2020).

[34] M. Abbasi, W. Chen, M. Naghiloo, Y. N. Joglekar, and K. W. Murch, Topological quantum state control through exceptional-point proximity, Phys. Rev. Lett. **128**, 160401 (2022).

[35] S. Khandelwal, N. Brunner, and G. Haack, Signatures of exceptional points in a quantum thermal machine, PRX Quantum **2**, 040346 (2021).

[36] J. W. Zhang, J. Q. Zhang, G. Y. Ding, J. C. Li, J. T. Bu, B Wang, L. L. Yan, S. L. Su, L. Chen, F. Nori *et al.*, Dynamical control of quantum heat engines using exceptional points, Nat. Commun. **13**, 6225 (2022).

[37] B. A. Tay, Liouvillian exceptional points in continuous variable system, Physica A **620**, 128736 (2023).

[38] F. Yang, P. Molignini, and E. J. Bergholtz, Dissipative boundary state preparation, arXiv:2305.00031.

[39] S. Machnes, M. B. Plenio, B. Reznik, A. M. Steane, and A. Retzker, Superfast laser cooling, Phys. Rev. Lett. **104**, 183001 (2010).

[40] J. Wiersig, Robustness of exceptional-point-based sensors against parametric noise: The role of Hamiltonian and Liouvillian degeneracies, Phys. Rev. A **101**, 053846 (2020).

[41] L. J. Fernández-Alcázar, R. Kononchuk, and T. Kottos, Thermal motors with enhanced performance due to engineered exceptional points, arXiv:2010.06743.

[42] G. Lindblad, On the generators of quantum dynamical semigroups, Commun. Math. Phys. **48**, 119 (1976).

[43] V. Gorini, A. Kossakowski, and E. C. G. Sudarshan, Completely positive dynamical semigroups of N-level systems, J. Math. Phys. **17**, 821 (1976).

[44] D. Huybrechts, F. Minganti, F. Nori, M. Wouters, and N. Shammah, Validity of mean-field theory in a dissipative critical system: Liouvillian gap, $\mathbb{PT}$-symmetric antigap, and permutational symmetry in the *XYZ* model, Phys. Rev. B **101**, 214302 (2020).

[45] T. Can, V. Oganesyan, D. Orgad, and S. Gopalakrishnan, Spectral gaps and midgap states in random quantum master equations, Phys. Rev. Lett. **123**, 234103 (2019).

[46] V. V. Albert and L. Jiang, Symmetries and conserved quantities in Lindblad master equations, Phys. Rev. A **89**, 022118 (2014).

[47] P. Zanardi and L. Campos Venuti, Geometry, robustness, and emerging unitarity in dissipation-projected dynamics, Phys. Rev. A **91**, 052324 (2015).

[48] P. M. Harrington, E. J. Mueller, and K. W. Murch, Engineered dissipation for quantum information science, Nat. Rev. Phys. **4**, 660 (2022).

[49] Y. Liu, S. Shankar, N. Ofek, M. Hatridge, A. Narla, K. M. Sliwa, L. Frunzio, R. J. Schoelkopf, and M. H. Devoret, Comparing and combining measurement-based and driven-dissipative entanglement stabilization, Phys. Rev. X **6**, 011022 (2016).

[50] Y. Lu, S. Chakram, N. Leung, N. Earnest, R. K. Naik, Z. Huang, P. Groszkowski, E. Kapit, J. Koch, and D. I. Schuster, Universal stabilization of a parametrically coupled qubit, Phys. Rev. Lett. **119**, 150502 (2017).

[51] K. W. Murch, U. Vool, D. Zhou, S. J. Weber, S. M. Girvin, and I. Siddiqi, Cavity-assisted quantum bath engineering, Phys. Rev. Lett. **109**, 183602 (2012).

[52] Y. Lin, J. P. Gaebler, F. Reiter, T. R. Tan, R. Bowler, A. S. Sørensen, D. Leibfried, and D. J. Wineland, Dissipative production of a maximally entangled steady state of two quantum bits, Nature (London) **504**, 415 (2013).

[53] B. Kraus, H. P. Büchler, S. Diehl, A. Kantian, A. Micheli, and P. Zoller, Preparation of entangled states by quantum Markov processes, Phys. Rev. A **78**, 042307 (2008).

[54] W.-C. Wang, Y.-L. Zhou, H.-L. Zhang, J. Zhang, M.-C. Zhang, Y. Xie, C.-W. Wu, T. Chen, B.-Q. Ou, W. Wu *et al.*, Observation of $\mathcal{PT}$-symmetric quantum coherence in a single-ion system, Phys. Rev. A **103**, L020201 (2021).

[55] D. C. Cole, S. D. Erickson, G. Zarantonello, K. P. Horn, P.-Y. Hou, J. J. Wu, D. H. Slichter, F. Reiter, C. P. Koch, and D. Leibfried, Resource-efficient dissipative entanglement of two trapped-ion qubits, Phys. Rev. Lett. **128**, 080502 (2022).

[56] C. Roos, T. Zeiger, H. Rohde, H. C. Nägerl, J. Eschner, D. Leibfried, F. Schmidt-Kaler, and R. Blatt, Quantum state engineering on an optical transition and decoherence in a paul trap, Phys. Rev. Lett. **83**, 4713 (1999).

[57] Z. Lin, A. Pick, M. Lončar, and A. W. Rodriguez, Enhanced spontaneous emission at third-order dirac exceptional points in inverse-designed photonic crystals, Phys. Rev. Lett. **117**, 107402 (2016).

[58] M. Partanen, J. Goetz, K. Y. Tan, K. Kohvakka, V. Sevriuk, R. E. Lake, R. Kokkoniemi, J. Ikonen, D. Hazra, A. Mäkinen *et al.*, Exceptional points in tunable superconducting resonators, Phys. Rev. B **100**, 134505 (2019).

[59] M. Naghiloo, M. Abbasi, Y. N. Joglekar, and K. W. Murch, Quantum state tomography across the exceptional point in a single dissipative qubit, Nat. Phys. **15**, 1232 (2019).

[60] X.-D. Dai, F. Song, and Z. Wang, Solvable BCS-Hubbard Lindbladians in arbitrary dimensions, Phys. Rev. B **108**, 115127 (2023).

[61] A. Kofman and G. Kurizki, Acceleration of quantum decay processes by frequent observations, Nature (London) **405**, 546 (2000).

[62] B. Misra and E. C. G. Sudarshan, The Zeno's paradox in quantum theory, J. Math. Phys. **18**, 756 (1977).

[63] M. C. Fischer, B. Gutiérrez-Medina, and M. G. Raizen, Observation of the quantum Zeno and anti-Zeno effects in an unstable system, Phys. Rev. Lett. **87**, 040402 (2001).

[64] T. Chen, W. Gou, D. Xie, T. Xiao, W. Yi, J. Jing, and B. Yan, Quantum Zeno effects across a parity-time symmetry breaking transition in atomic momentum space, npj Quantum Inf. **7**, 78 (2021).

[65] P. Facchi, H. Nakazato, and S. Pascazio, From the quantum Zeno to the inverse quantum Zeno effect, Phys. Rev. Lett. **86**, 2699 (2001).

[66] J. Li, T. Wang, L. Luo, S. Vemuri, and Y. N. Joglekar, Unification of quantum Zeno-anti Zeno effects and parity-time symmetry breaking transitions, Phys. Rev. Res. **5**, 023204 (2023).

[67] F. Reiter and A. S. Sørensen, Effective operator formalism for open quantum systems, Phys. Rev. A **85**, 032111 (2012).

[68] S. Haroche and J.-M. Raimond, *Exploring the Quantum Atoms, Cavities, and Photons* (Oxford University Press, Oxford, 2010), pp. 205–206.

[69] J. Bechhoefer, A. Kumar, and R. Chétrite, A fresh understanding of the Mpemba effect, Nat. Rev. Phys. **3**, 534 (2021).

[70] H. Jing, Ş. K. Özdemir, H. Lü, and F. Nori, High-order exceptional points in optomechanics, Sci. Rep. **7**, 3386 (2017).

[71] J. Li, A. K. Harter, J. Liu, L. de Melo, Y. N. Joglekar, and L. Luo, Observation of parity-time symmetry breaking transitions in a dissipative Floquet system of ultracold atoms, Nat. Commun. **10**, 855 (2019).

[72] K. Szczygielski, On the application of Floquet theorem in development of time-dependent Lindbladians, J. Math. Phys. **55**, 083506 (2014).

[73] M. Hartmann, D. Poletti, M. Ivanchenko, S. Denisov, and P. Hänggi, Asymptotic Floquet states of open quantum systems: The role of interaction, New J. Phys. **19**, 083011 (2017).

[74] A. Schnell, S. Denisov, and A. Eckardt, High-frequency expansions for time-periodic Lindblad generators, Phys. Rev. B **104**, 165414 (2021).

[75] J. Gunderson, J. Muldoon, K. W. Murch, and Y. N. Joglekar, Floquet exceptional contours in Lindblad dynamics with time-periodic drive and dissipation, Phys. Rev. A **103**, 023718 (2021).

[76] C. Cohen-Tannoudji, *Atom-Photon Interactions* (Wiley-VCH Verlag GmbH & Co. KGaA, Weinheim, 2004).